

A COMPARISON OF WEAK LENSING MEASUREMENTS FROM GROUND- AND SPACE-BASED FACILITIES

MANSI M. KASLIWAL^{1,2}, RICHARD MASSEY¹, RICHARD S. ELLIS¹, SATOSHI MIYAZAKI³ & JASON RHODES^{4,1}

Draft version October 29, 2018

ABSTRACT

We assess the relative merits of weak lensing surveys, using overlapping imaging data from the ground-based Subaru telescope and the Hubble Space Telescope (HST). Our tests complement similar studies undertaken with simulated data. From observations of 230,000 matched objects in the 2 square degree COSMOS field, we identify the limit at which faint galaxy shapes can be reliably measured from the ground. Our ground-based shear catalog achieves sub-percent calibration bias compared to high resolution space-based data, for galaxies brighter than $i' \simeq 24.5$ and with half-light radii larger than $1.8''$. This selection corresponds to a surface density of 15 galaxies arcmin⁻² compared to ~ 71 arcmin⁻² from space. On the other hand the survey speed of current ground-based facilities is much faster than that of HST, although this gain is mitigated by the increased depth of space-based imaging desirable for tomographic (3D) analyses. As an independent experiment, we also reconstruct the projected mass distribution in the COSMOS field using both data sets, and compare the derived cluster catalogs with those from X-ray observations. The ground-based catalog achieves a reasonable degree of completeness, with minimal contamination and no detected bias, for massive clusters at redshifts $0.2 < z < 0.5$. The space-based data provide improved precision and a greater sensitivity to clusters of lower mass or at higher redshift.

Subject headings: cosmology: observations – gravitational lensing – instrumentation

1. INTRODUCTION

Dark matter dominates the gravitational component of the cosmic energy density and thus provides the framework for structure formation in the Universe. However, by its nature, the distribution and cosmic growth are challenging to observe. The most promising probe is weak gravitational lensing: analysis of the distorted shapes of ordinary galaxies behind foreground mass concentrations. Several numerical techniques are now available to recover the projected mass distribution from these distortions, and tests on simulated datasets are underway to verify their precision (Heymans et al. 2005a; Massey et al. 2007c). There is great optimism in the weak lensing community that such methods will enable both the tomographic mapping of dark matter structures in time and space. This will also provide a robust statistical measure of the nature of dark energy over redshifts $0 < z < 1$ (Mellier 1999; Refregier 2003)

Observational progress has been particularly dramatic. The first detections of statistical “cosmic shear” were only published in 2000 (Bacon, Refregier & Ellis 2000; Kaiser et al. 2000; Wittman et al. 2000; van Waerbeke et al. 2000). In the subsequent seven years, weak lensing surveys have measured the dark matter power spectrum (Brown et al. 2003; Heymans et al. 2005b; Hoekstra et al. 2006; Semboloni et al. 2006), traced the evolution of structure (Bacon et al. 2005;

Kitching et al. 2007; Massey et al. 2007a), enabled the construction of lensing-selected cluster catalogs (Miyazaki et al. 2002a; Wittman et al. 2006; Schirmer et al. 2007; Miyazaki et al. 2007), and non-parametrically reconstructed the total mass distribution both in clusters (Kneib et al. 2003; Clowe et al. 2006; Jee et al. 2007a) and on larger scales (Massey et al. 2007b). As a result, weak lensing has been identified as the most promising route to understanding the nature of dark energy by the ESA-ESO Working Group on Fundamental Cosmology⁵, joint NSF-NASA-DOE Astronomy and Astrophysics Advisory Committee⁶, and NSF-DOE High Energy Physics Advisory Panel Dark Energy Task Force⁷.

The primary signal of any weak lensing analysis is the statistically coherent distortion of background galaxies along adjacent lines of sight. The main sources of statistical noise are the finite density of galaxies that can be sufficiently well-detected and resolved for accurate shape measurement, plus their intrinsic morphologies. The density of resolved galaxies also governs the angular resolution and fidelity of a reconstructed mass map which, in turn, determines the limiting halo mass that can be detected. On the other hand, statistical analyses of the dark matter power spectrum are less concerned with individual halos but require panoramic fields to counter the effects of cosmic (sample) variance. Minimizing statistical errors in such an analysis, within a finite survey lifetime, requires an optimal balance between area and depth.

A key debate in the development of future weak lensing experiments concerns the relative merits of ground- ver-

¹ Astronomy Department, California Institute of Technology, 105-24, Pasadena, CA 91125, USA

² George Ellory Hale Fellow of Moore Foundation

³ National Astronomical Observatory of Japan, Mitaka, Tokyo 181-8588, Japan

⁴ Jet Propulsion Laboratory, California Institute of Technology, 105-24, Pasadena, CA 91125, USA

⁵ http://www.stecf.org/coordination/esa_eso/cosmology.php

⁶ <http://www.nsf.gov/mps/ast/aaac.jsp>

⁷ <http://www.nsf.gov/mps/ast/detf.jsp>

sus space-based platforms. Ambitious surveys now being planned with dedicated, ground-based facilities (eg VST-KIDS, DES, Pan-STARRS, LSST). These are driven by technological progress including panoramic cameras with small optical distortions, highly sensitive imaging detectors, and (in the case of Pan-STARRS) on-chip active correction to reduce the width of the point spread function (PSF). Future surveys spanning significant fractions of the celestial sphere are envisaged, promising tight constraints on the cosmological parameters.

However, measurements with current ground-based facilities are limited by the size and temporal variations of the PSF. There is concern in many quarters that wide-field facilities operating in space (e.g. DUNE, SNAP, JDEM) will ultimately be required to achieve the precision required (particularly) to distinguish between various models of dark energy. Space-based facilities will be more costly but will likely offer increased depth, better photometric performance and a stable PSF. The key issue in gauging their merits is not statistical error, but the extent to which potential biases in ground-based data may act as a “systematic floor” to prevent complete exploitation.

Some valuable answers can be obtained by comparing simulated ground and space-based images, (Wittman 2005; Lampton et al. 2006) and the Shear TESting Programme (STEP: Heymans et al. 2005a; Massey et al. 2007c). However, the input parameters used to generate the simulated data may not be realistic or address all the instrumental idiosyncrasies. Of particular concern are the stability and vagaries of the PSF. No simulations have yet adequately addressed this point – which may, ultimately, be the limiting problem for ground-based data. It is often argued that future facilities will be carefully designed to mitigate any limitations realized with current observational facilities. While progress can no doubt be expected, both on the ground and in space, we believe many lessons can be learned from extant data and hardware with proven engineering pedigree.

In this paper, we present the first direct comparison of weak lensing analysis *for the same sky field* using ground and space-based data. Deep, panoramic imaging has been obtained for the 1.64 deg^2 COSMOS field (Scoville et al. 2007a) by both the Advanced Camera for Surveys (ACS) on board the Hubble Space Telescope (HST) (Scoville et al. 2007b) and the *Suprime-Cam* imager at the prime focus of the Subaru 8.2m telescope (Taniguchi et al. 2007a). In both cases, the entire field was covered by mosaicing many independent exposures. The SuPrimeCam instrument was constructed with weak lensing analysis particularly in mind, and currently provides the best image performance available from any ground-based telescope, in terms of optical distortions over a large field. A comparison of these datasets should therefore provide a realistic and valuable assessment of the relative performance of state-of-the-art imagers on the ground and in space.

The paper is organized as follows. In §2, we briefly review the relevant theory. In §3, we describe the two data sets, data reduction pipelines and weak lensing analyses. We then present the results. In §4, we compare shear measures on a galaxy-by-galaxy basis to determine the optimum depth at which the ground-based data matches

the performance of the (deeper) space based data. This permits us to determine the relative survey speeds of Subaru and HST for high precision cosmic shear experiments. In §5, we construct maps of the mass distribution, treating the Subaru and HST maps as independent probes of the same field, and contrast these against X-ray data. This permits us to evaluate the completeness and reliability of a lensing-selected halo catalog, and evaluate the precision of their inferred masses as a function of redshift. In §6, we summarize our results and discuss their wider implications for future missions.

2. REVIEW OF WEAK LENSING THEORY

Gravitational lensing by foreground mass structures distorts an image plane of distant galaxies $I(\mathbf{x})$ via a coordinate transformation

$$\mathcal{A}_{ij} = \delta_{ij} + \frac{\partial(\delta x_i)}{\partial x_j} = \begin{pmatrix} 1 - \kappa - \gamma_1 & \gamma_2 \\ \gamma_2 & 1 - \kappa + \gamma_1 \end{pmatrix}, \quad (1)$$

where $\delta x_i(\mathbf{x})$ is the deflection angle of the light rays. The *convergence*

$$\kappa(\mathbf{x}) = \frac{4\pi G}{2c^2} \int g(z) \rho(\mathbf{x}, z) dz, \quad (2)$$

describes overall dilations and contractions. It is proportional to the total mass density ρ projected along a line of sight, where the *lensing sensitivity function*

$$g(z) = \frac{2D_L D_{LS}}{D_S} \quad (3)$$

reflects the efficiency of foreground gravitational lenses at different redshifts – containing a ratio of the angular diameter distance to a lens, the background source, and between the two. This can be more simply written as

$$\kappa \equiv \frac{1}{2} \left(\frac{\partial^2 \Psi}{\partial x^2} + \frac{\partial^2 \Psi}{\partial y^2} \right), \quad (4)$$

in terms of a 2D, projected version $\Psi(\mathbf{x})$ of the Newtonian gravitational potential. Two components of *shear*

$$\{\gamma_1, \gamma_2\} \equiv \left\{ \frac{1}{2} \left(\frac{\partial^2 \Psi}{\partial x^2} - \frac{\partial^2 \Psi}{\partial y^2} \right), \frac{\partial^2 \Psi}{\partial x \partial y} \right\}, \quad (5)$$

describe stretches and compressions along (at 45° from) the x -axis.

The observed shapes of background galaxies can be described by combination of their Gaussian-weighted quadrupole moments

$$d \equiv \frac{\iint I(\mathbf{x}) W(\mathbf{x}) r^2 d^2 \mathbf{x}}{\iint I(\mathbf{x}) W(\mathbf{x}) d^2 \mathbf{x}}, \quad (6)$$

$$\{\varepsilon_1, \varepsilon_2\} \equiv \frac{\iint I(\mathbf{x}) W(\mathbf{x}) r^2 (\cos(2\theta), \sin(2\theta)) d^2 \mathbf{x}}{\iint I(\mathbf{x}) W(\mathbf{x}) r^2 d^2 \mathbf{x}}, \quad (7)$$

where

$$W(\mathbf{x}) = e^{-r^2/2r_g^2}. \quad (8)$$

Although κ is generally the desired quantity, and could be obtained in principle from measurements of galaxy sizes (6) or fluxes, this has proved difficult in practice, because expectations for these quantities prior to lensing

are unknown. On the other hand, while galaxies have a natural dispersion of intrinsic ellipticities (7), they are (almost) uncorrelated with each other in the absence of lensing, i.e. $\langle \varepsilon_i \rangle = 0$. Any correlation between the *observed* ellipticities of galaxies seen along adjacent lines of sight arises because their light has traversed similar intervening large-scale structure $\rho(\mathbf{x}, z)$. In practice, corrections to measured ellipticities also need to be made for the smearing of galaxies by the PSF, and for the differing susceptibilities of some galaxy morphologies to an input shear. For more details of this procedure, see e.g. (Kaiser, Squires & Broadhurst 1995).

The observed shear can finally be transformed into convergence through their close relation in Fourier space

$$\tilde{\kappa} = \frac{(\ell_1^2 - \ell_2^2)\tilde{\gamma}_1 + (2\ell_1\ell_2)\tilde{\gamma}_2}{(\ell_1^2 + \ell_2^2)} \quad (9)$$

(Kaiser & Squires 1993). This is typically some amount, to reduce noise. Furthermore, like any scalar quantity extracted from a vector field, a convergence signal can also be split into two independent components, $\kappa = \kappa^E + i \kappa^B$ (King & Schneider 2001). The grad-like “*E*-mode” is the signal produced by weak lensing. The curl-like “*B*-mode” is not produced by physical processes (except at very low levels, as described by Schneider et al. 2002), and therefore ought to be consistent with zero in the absence of systematics. Usefully, it contains the same noise properties as the *E*-mode signal – so it acts as an independent realization of noise in the field, and any significant deviations from zero alert to the presence of residual systematics (such as imperfect correction for the PSF).

3. OBSERVATIONS AND DATA REDUCTION

3.1. The COSMOS Data Sets

Our data all cover the COSMOS survey field, a 1.64 deg^2 contiguous square, centered at 10:00:28.6, +02:12:21.0 (J2000) (Scoville et al. 2007a). The ground-based imaging was obtained in eleven mosaiced pointings of the *Suprime-Cam* camera at the prime focus of the Subaru telescope on Mauna Kea (Miyazaki et al. 2002b). These were taken on the 18th and 21st of February 2004, nights selected for their excellent observing conditions: the mean seeing was $0.54'' \pm 0.03''$. The field constitutes part of a larger weak lensing survey discussed, along with full details of the primary data reduction pipeline, in (Miyazaki et al. 2007, Green et al. *in prep.*). In fact, the relevant field in that survey covered a slightly larger area than the COSMOS field. The Subaru imaging was truncated *after* making convergence maps, to avoid edge effects associated with the Fourier transform operations in equation (9).

Our comparison is made possible by the unique availability of deep, panoramic space-based imaging of the COSMOS field (Scoville et al. 2007b). During HST cycles 13 and 14, 577 slightly overlapping pointings were obtained from the *Advanced Camera for Surveys* (ACS) on board the Hubble Space Telescope. Four dithered exposures at each pointing were stacked using the DRIZZLE algorithm (Fruchter & Hook 2002) to improve the native pixel scale of $0.05''$ and recover a final pixel scale of $0.03''$. Full details of the primary data reduction pipeline for the HST images are given in (Koekemoer et al. 2007).

It is important to emphasize that both the *ACS* and *Suprime-Cam* data exhibit idiosyncrasies that present significant challenges for weak lensing analysis. For example, the atmospheric seeing varied during the two nights over which the Subaru data were obtained; and the distortions of the telescope’s primary mirror under a gravity load were only passively corrected via a look-up table as it followed the field. In a future ground-based experiment, such as LSST or Pan-STARRS, seeing variations could be normalized over a survey by stacking a very large number of short, independent exposures taken over a long time period. Dome seeing could likewise be improved with future technologies. And while the telescope superstructure is particularly rigid at Subaru, active correction of the mirror support could undoubtedly improve future designs. Equivalently, the sky background seen from HST is affected by Earthshine that depends on the telescope pointing (Leauthaud et al. 2007). The HST PSF also varies over time due to thermal fluctuations during each low-Earth orbit (Jee et al. 2007a; Rhodes et al. 2007). Finally, the charge transfer efficiency of the *ACS* CCD detectors had been significantly degraded by high energy particles by the time the COSMOS data were obtained, and worsened during the observing window (Rhodes et al. 2007). None of these problems are inherent to all space-based observations: future missions might minimize or eliminate all three effects by adopting a regular observing pattern, orbiting the Lagrange point L2, and using radiation-hardened CCDs. However, the weak lensing analysis of existing space-based data is indeed compromised by the extent to which such hardware variations can be modeled. In this sense, our comparison is actually more informative than one based on simulated data that reproduces only idealized and mean instrumental characteristics.

The relevant characteristics of the two data sets are summarized in Table 1, including limiting depths for a point source at 5σ , in a $3''$ aperture from the ground and a $0.15''$ aperture from space (Capak et al. 2007). In addition to these images, the COSMOS field has been observed across all wavelengths from radio to X-rays. Of particular relevance here are (i) deep X-ray observations by XMM (Hasinger et al. 2007), which can be used to locate massive structures via thermal emission from hot gas; and (ii) multicolor optical and near-IR imaging campaigns from the Subaru, Canada France Hawaii, Cerro Tololo and Kitt Peak telescopes, which provide 15 additional bands and photometric redshifts (Capak et al. 2007; Mobasher et al. 2007). The photometric redshift estimation code uses Bayesian priors based on an adopted luminosity function, and includes reddening based on both Galactic and Calzetti extinction laws. The results were calibrated using 868 galaxies in the field brighter than $i' = 24$ and with spectroscopic redshifts. For galaxies closer than $z = 1.2$, the rms scatter in $(z_{\text{phot}} - z_{\text{spec}}) / (1 + z_{\text{spec}})$ is 0.031.

3.2. Object Detection

Objects were detected in the Subaru images using HFINDPEAKS from the IMCAT package⁸. This finds the centroid and scale size r_g that maximizes the peak S/N

⁸ Nick Kasiser’s *imcat* software package is available from <http://www.ifa.hawaii.edu/~kaiser/imcat/>

TABLE 1
SURVEY CHARACTERISTICS

	Ground	Space
Instrument	Subaru/ <i>Suprime-Cam</i>	HST/ <i>ACS</i>
Primary aperture	8.2m	2.4m
Exposure time	5×360 s	4×507 s
Total survey time	5 hours	325 hours
Filter	i'	F814W
Limiting AB magnitude	26.2	26.6
Field of View	2.14 deg^2	1.67 deg^2
Pixel Scale	$0.202''$	$0.03''$
Point Spread Function	$0.68''$	$0.12''$

of the image after smoothing with a Gaussian. The code also returns the half-light radius, r_h , of each galaxy. Galaxies were initially detected to magnitudes fainter than those for which it is possible to accurately measure shapes. To reduce noise in the final analysis, weights were given to each galaxy, and galaxies with a detection $S/N < 14$ were removed from the catalog altogether. The resulting surface density is $n_{\text{gal}} = 42 \text{ galaxies arcmin}^{-2}$.

Objects were detected in the *ACS* images using SExtractor (Bertin & Arnouts 1996) in a dual Hot/Cold configuration (Leauthaud et al. 2007), designed to identify both large and small objects while avoiding fragmentation of the former, or merging of the latter. The SExtractor centroids were then improved, and the best-fitting scale size was selected, via an iterative process during shape measurement. Galaxies smaller than $d = 0.11''$ or fainter than $S/N \approx 20$ were removed from the catalog, and a weighting scheme was applied to faint galaxies as a function of their detection S/N (Leauthaud et al. 2007). Note that an absolute calibration of the S/N was difficult to determine in practice, because flux in adjacent pixels becomes correlated during DRIZZLE. The S/N cut corresponds approximately to a limiting magnitude $F814W(AB) < 26.5$ for a point source. The resulting surface density is $n_{\text{gal}} = 71 \text{ galaxies arcmin}^{-2}$, with a median redshift $z_{\text{med}} = 1.2$.

3.3. Shear Measurement

Because the image characteristics of the two data sets are quite different, we adopted separate methods to measure galaxy shapes, remove PSF effects, and ultimately obtain the weak lensing shear signal. Each of these methods has been optimized for the respective data sets, so our comparison will necessarily incorporate the limitations of each pipeline. We believe this is in the spirit of a fair comparison of ground versus space. To minimize any differences arising entirely from the algorithms themselves however, we have intentionally adopted related methods from the same generation of software development and codes that have been well-tested. Although newer shear measurement methods (Kaiser 2000; Bridle et al. 2001; Dahle et al. 2002; Refregier & Bacon 2003; Bernstein & Jarvis 2002; Hirata & Seljak 2003; Kuijken 2006; Massey et al. 2007d; Nakajima & Bernstein 2007) may offer improved performance, none has yet been sufficiently tested across both observing regimes.

The Subaru images were analyzed with the (Hamana et al. 2003) implementation of the widely used (Kaiser, Squires & Broadhurst 1995, hereafter

KSB) shear measurement method. This particular implementation is a derivative of the “LV” pipeline tested in the Shear TEsting Program (Heymans et al. 2005a; Massey et al. 2007c).

The HST images were analyzed with the (Rhodes et al. 2001, hereafter RRG) shear measurement method. This is a perturbation of the KSB method for space-based data. It calculates the same quadrupole moments, but corrects them individually for the effects of convolution with the PSF, and only in the final stage takes the ratio (7). This is necessary because the small and cuspy diffraction-limited PSFs otherwise introduce divisions by very small (and noisy) numbers. RRG been applied to HST *WFPC2* (Rhodes et al. 2001), *STIS* (Rhodes et al. 2004), and *ACS* data (Massey et al. 2007a). The *ACS* pipeline was thoroughly tested on simulated images during the creation of the COSMOS catalog (Leauthaud et al. 2007), and also for a continuation of STEP using simulated space-based images.

4. STATISTICAL APPLICATIONS

4.1. Shear-shear comparisons

We shall now compare the global properties of our ground- and space-based shear catalogs, to determine the depth (and galaxy surface density) at which reliable shear measurement is possible from the ground. This will be relevant for many statistical applications, including measurements of the angular shear-shear correlation function that are typically used to constrain cosmological parameters. In such analyses, where statistical noise is reduced by averaging over many lines of sight, the key issue is the reliability and level of residual systematics in the shear measurement.

We assess the performance of the ground-based shear measurements against those from *the same galaxies* in space-based data, making the necessary but reasonable assumption that the shapes are much more reliable when measured from the much higher resolution images with a smaller PSF. Such a comparison is clearly only possible for the subset of galaxies contained in both catalogs. The two quantities of interest will be linearity in the comparison (the slope of the shear-shear comparison is equivalent to the STEP “calibration bias” parameter m) and the scatter (which represents the combined shear measurement noise from both HST and Subaru, plus any systematic effects).

We match galaxies whose positions agree to within $1''$, and produce a common catalog containing $n_{\text{gal}} = 32 \text{ galaxies arcmin}^{-2}$. Many objects in the Subaru galaxy catalog without matched counterparts in HST galaxy catalog have half-light radii on the limits of seeing and are likely to have been revealed as stars by the higher resolution data; in any case, the omitted galaxies had below-average weights in the Subaru catalog. The remaining unmatched objects are a combination of noisy/skewed galaxies with offset centroids, or galaxies that lie in regions of the HST images masked because of scattered light from nearby bright stars. For the following tests, we shall ignore the weights on remaining galaxies, and treat all objects equally.

Figure 1 shows a comparison of the shear signal for the matched galaxies. Since errors are present in both

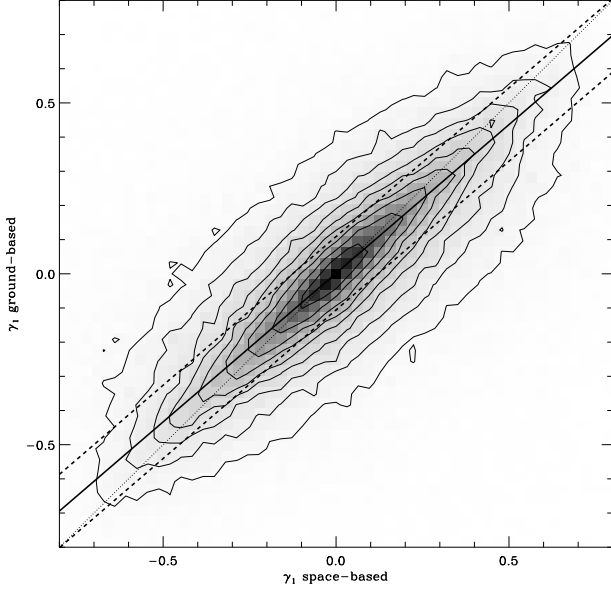


FIG. 1.— Comparison of shear measured from galaxies seen in both Subaru and Hubble Space Telescope images. The greyscale shows the number of galaxies with different shear measurements. The outer contour includes 90% of the galaxies, and successive inner ones include 10% fewer. The solid line is the least squares linear relation. Its slope of 0.87 indicates that shears have been underestimated in the ground-based analysis, or that the catalog is still partially contaminated by stellar sources. This value is insensitive within 0.01 to the reintroduction of galaxy weights. Furthermore, the non-Gaussian wings of the scatter extend well beyond the rms error of 0.16, shown as dashed lines.

axes, to calculate the best-fit linear relationship we adopt a least squares method that minimizes the perpendicular distance to the best fit line (instead of one that assumes one variable is error-free). Ideal shear measurement from both instruments would yield a best-fit slope of unity. There will inevitably be a small amount of scatter, because the weight function (8) is not necessarily the same size r_g in the ground- and space-based analyses. In practice, we find a best-fit slope of 0.87, indicating that the shears have been underestimated from the ground. The measurement noise is also problematic, with $\sigma_\gamma = 0.16$ per component (perpendicular to the best-fit line; note that this does not include intrinsic source ellipticity variance because the galaxies are matched) and a skewed, non-Gaussian distribution of outlying shear estimates that would render a cosmic shear analysis less stable.

The overall performance in figure 1 is a superposition of good shears from bright and (in particular) large galaxies, plus smaller objects that cause most of the bias and scatter. Indeed, systematic errors could be completely eliminated by using only the very largest galaxies. However, the statistical noise in a cosmic shear analysis of shear-shear correlation functions scales as $\sigma_\gamma/\sqrt{n_{\text{gal}}}$. An optimal strategy for any particular ground-based survey will involve catalog cuts requiring a trade-off between systematic and statistical errors. However, the optimal cuts will vary as a function of survey area and depth. To produce a result of general interest, we therefore show in Figures 2 and 3, the resulting calibration bias, scatter and galaxy density for a range of possible cuts in galaxy size and magnitude.

A simple result emerges from Figure 2. It is notice-

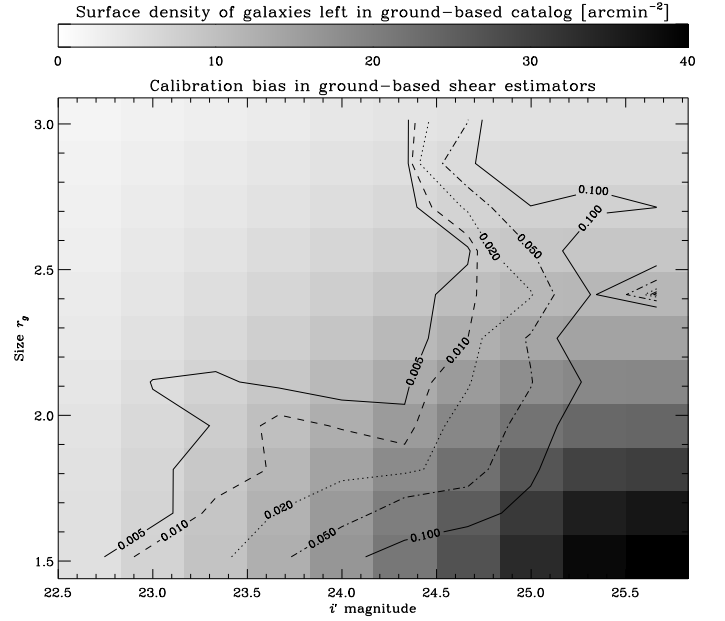


FIG. 2.— Relative calibration between shear measurements from galaxies in Subaru and Hubble Space Telescope data, for galaxies of different sizes and magnitudes. The contours show deviations from a slope of unity in figures 1 and 4, which would have been ideal. For faint galaxies, these deviations tended to be an underestimation in the Subaru pipeline relative to HST. There is some evidence that shears are overestimated in large, bright galaxies, although the small number of these objects means that the extrapolation is less certain. The calibration biases are calculated locally, for galaxies only in a given cell of {size,magnitude} space. On the other hand, the grey-scale shows the cumulative number density of galaxies n_{gal} that would remain in a ground-based catalog, were cuts to be applied at the local values (i.e. including all larger and brighter galaxies).

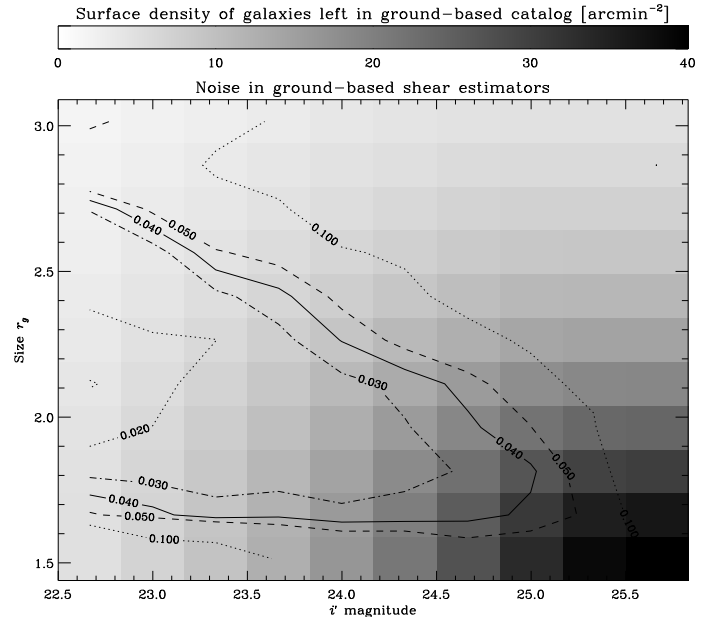


FIG. 3.— Combined noise from shear measurements of galaxies matched in catalogs from Subaru and Hubble Space Telescope data. The contours show σ_γ as a function of galaxy size and magnitude. As in figure 2, these are calculated only for galaxies with that particular size and magnitude. The contours close at the top merely because there are very few large, faint galaxies, so the rms scatter increases. The grey scale again shows the total number density of available galaxies.

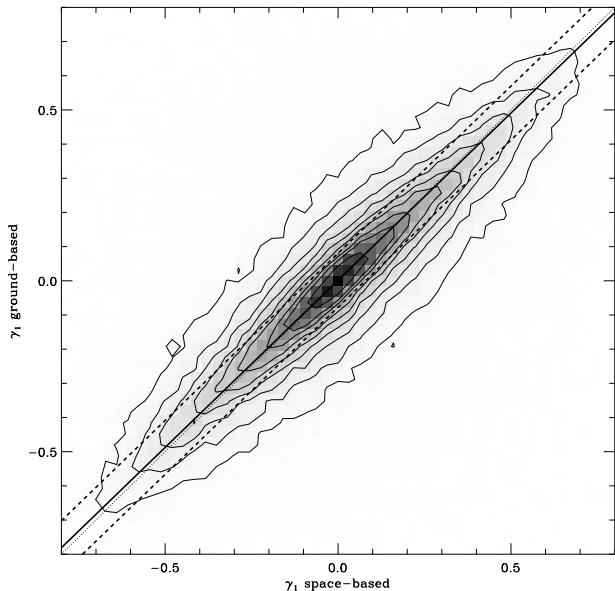


FIG. 4.— As for figure 1, but for the subset of galaxies brighter than $i' = 24.5$ and larger than $r_h = 1.8''$. The total least squares slope is 0.97, implying an almost unbiased recovery of the shear signal from Subaru, and the data is better and more symmetrically enclosed within the rms scatter of 0.11.

able from the horizontal and vertical contours that size and magnitude cuts seem to neatly parametrize independent sources of error. Using existing shape measurement methodology, shear can be measured from galaxies brighter than $i' = 24.5$ and larger than $r_h = 1.8$, with measurement noise $\sigma_\gamma \simeq 0.03$ and a calibration bias less than 3% (and only 1% with galaxy weighting), which is acceptable for competitive constraints from future surveys (Refregier et al. 2004). This leaves a surface density of $n_{\text{gal}} = 15$ galaxies arcmin² from the ground, with a median redshift of $z_{\text{med}} = 0.8$. The comparison with space-based data for these cuts is shown in figure 4.

Note that we have not been able to test the reliability of space-based shear measurements using this method, nor even considered the population of small galaxies resolved only from space. Without data even better than *ACS* imaging to compare to, we resort to simulations. The full RRG pipeline was calibrated against simulated images by (Leauthaud et al. 2007). However, of the 71 galaxies arcmin² successfully in real *ACS* images, only the brightest 40 could be used by (Massey et al. 2007a) to minimize the *B*-mode signal and overcome problems of CCD charge transfer inefficiency (CTI). This limitation clearly needs to be overcome: perhaps via a CTI correction algorithm like that developed for *STIS* by (Bristow et al. 2004), and radiation-hardened detectors in future telescopes.

4.2. Survey speed

Our ground versus space shear comparisons have important implications when it comes to considering the optimal approach for measuring shear for cosmological applications. Although the *étendue* of instruments can be expected to increase both on the ground and in space, we will base our discussion on the imaging depth and fields of view of our HST and Subaru surveys.

An important criterion is what can be accomplished in a given amount of observing time; the HST and Sub-

aru requirements for our comparison are summarized in Table 1). HST overheads approximately tripled the on-source exposure time, and, at Subaru, high quality imaging was secured during what might be considered a fortuitous observing window. Noting that (Bacon et al. 2001) found images with seeing worse than $\sim 0.8''$ of little use for weak lensing analysis, coupled with observational visibility, it seems reasonable to incorporate a factor of at least four inefficiency for a generic survey: even for a superb ground-based facility such as Subaru, on an excellent site such as Mauna Kea⁹. Based on its superior field of view, Subaru is then ~ 24 times faster than HST in useful mapping speed. As, to first order, the signal to noise in statistical analyses increases as $\sqrt{n_{\text{gal}}}$, for a fixed survey lifetime, this corresponds to a ~ 5 -fold improvement in signal to noise.

This simplistic analysis is of course mitigated by the higher resolution available from space. We next insert the gain in surface density, viz 71 galaxies arcmin² resolved in our space-based imaging c.f. 15 arcmin² from the ground. We will assume that the additional, small galaxies have a similar distribution of intrinsic ellipticities as the larger ones (c.f. Massey et al. 2004; Leauthaud et al. 2007) and that the measurement noise on an average survey galaxy is constant (since the size distribution of resolved galaxies compared to the PSF size is roughly independent of the PSF size). Incorporating this increased background surface density, the ground-based gain per unit time drops to only a factor of 2.3.

Equally important to the increased density of galaxies are their higher redshifts. Distant galaxies are more sensitive to low-redshift lenses, and sensitive to more total lenses. The shear signal grows proportionally to the median source redshift $z_{\text{med}}^{0.6-0.8}$ (Jain & Seljak 1997). With the redshift distributions for galaxies shown in figure 5, the total gain in signal to noise for a 2D weak lensing survey conducted from Subaru over one conducted with HST is only about 1.7.

Perhaps the most important advantage of space is the increased redshift range of resolved galaxies. This better enables their stratification into redshift bins for tomographic (3D) analyses. Deep infrared imaging, needed for accurate photometric redshifts, is also likely to remain the province of space-based observatories. Tomographic techniques can tighten the constraints on cosmological parameters Ω_M and σ_8 by a factor of at least three (Massey et al. 2007a) and potentially as much as five (Heavens, Kitching & Taylor 2006). Further advantages of these techniques includes the elimination of unwanted signal from adjacent galaxies' intrinsically-correlated shapes (King & Schneider 2003; Heymans & Heavens 2003). While wide-field ground-based instruments may therefore yield significant improvements for Dark Energy Task Force “Stage 3” surveys, advanced analysis techniques for “Stage 4” surveys will realistically be possible only with space-based facilities. These will bring new scientific opportunities, cross-

⁹ <http://www.cfht.hawaii.edu/Instruments/Imaging/Megacam/observingstats.html>. Future surveys such as Pan-STARRS and LSST, which plan to co-add many short exposures with independent PSFs, may achieve near-uniform image quality by rejecting a certain fraction of exposures. But the relevant figure of merit is still the fraction of time spent with seeing better than $0.8''$.

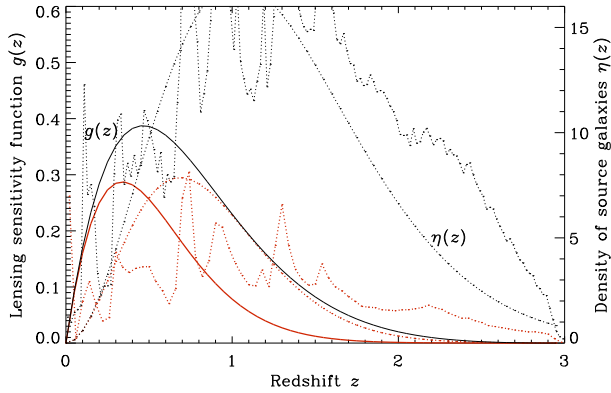


FIG. 5.— The dotted lines show the redshift distribution of source galaxies from Hubble Space Telescope (black) and Subaru (red) imaging surveys, for the catalog cuts used in figure 4. The jagged lines show the measured photo- z s, and the smooth curves assume a simple parametric form for the background galaxy redshift distribution from (Smail, Ellis & Fitchett 1994), with $\alpha = 2$, $\beta = 1.5$, $z_{\text{med}} = 0.8$ or 1.2 , and an overall normalization to reproduce the observed number density of galaxies. The solid lines show the corresponding lensing sensitivity functions calculated from the analytic curves. These lie always in front of the source galaxies but are notably higher for a space-based survey, particularly at redshifts greater than 0.5 . Extending this redshift coverage is crucial for 3D tomographic analysis techniques to measure the growth of structure.

checks for systematics, and greater efficiency.

5. MASS MAPS AND HALO DETECTION

We now investigate the reconstruction of maps of the mass distribution (figures 6 and 7), and the detection of individual mass peaks. The mass and redshift distribution $N(M, z)$ of several thousand lensing-selected clusters could be used to constrain cosmological models (Hamana et al. 2003; Wang et al. 2004, Green et al. *in prep.*). Additionally, the physical properties of the dark matter particles can be investigated by comparing the detailed distribution of dark matter with that of baryons (Clowe et al. 2006; Jee et al. 2007b). The key issues will be the angular resolution of reconstructed mass maps, as well as the mass and redshift range in which halos can be successfully detected. We treat this as an independent experiment from the previous section, beginning the comparison of ground- and space-based data afresh. In particular, we do *not* cut the Subaru data to the shallower depth discussed in §4.1, to eliminate the last few systematic biases. The intent is not to align our two comparisons but rather to optimize each analysis as an independent experiment – as would be the case if either were being undertaken as a self-contained survey.

Unfortunately, even with the unprecedented investment of HST time for the COSMOS survey, we can expect the number of lensing-detected structures in this finite field to be modest. At the Subaru depth, a surface density of ~ 5 halos deg^{-2} (Miyazaki et al. 2007) implies only around eight halos are likely to be found in the COSMOS field. Thus we recognize in this comparison that the statistical significance of our results will be quite limited.

5.1. Residual Systematics

First, we consider the B -mode signal. As discussed in §2, the B -modes act as an independent realization of noise in the mass map, and locally highlight any prob-

lems with the correction for PSF or other effects peculiar to the (two very different) instruments. Unsurprisingly, a visual inspection of Figure 7 shows that the B -mode signal is significantly lower in our space-based data, with fewer B -mode peaks. The overall noise level is reduced, and holes arising from masked foreground stars are also smaller and less frequent. In the ground-based maps, these create additional edges that lead to spurious effects during the Fourier transforms required by equation (9). The extended gaps are caused by difficulties modeling the PSF near the edge of the field of view, and could be eliminated in future surveys by more conservative tiling strategies.

The southwest corner of the field has been troublesome throughout our analysis. This pointing was observed in slightly worse seeing, so the density of galaxies is reduced and the noise in the mass reconstruction is higher.

5.2. Halo Detection

The higher surface density of background galaxies from space also improves the reconstruction of the E -mode “mass map” convergence field. The noise is lower and the angular resolution higher (although to aid comparison, both panels in figure 6 are smoothed to the same scale). Several of the key features are qualitatively similar but we are struck by the significant differences in the prominence of other mass peaks. To evaluate the robustness of detections, we shall now employ an automated peak-finding algorithm.

Following (Miyazaki et al. 2007), we smooth the convergence maps by a Gaussian kernel of rms width $1'$ and find local maxima with detection significance $\nu > 4$ (assuming Gaussian errors on the shear measured within $0.7'$ cells on the sky equal to the dispersion of those galaxy shears). Five peaks (marked A, B, C, D and K in figure 6) are then identified in the ground-based data. However, two of these are near boundaries of the field mask. Imposing the rigorous restrictions discussed by (Miyazaki et al. 2007), we find that only peaks A, B and C remain (c.f. table 3 in Miyazaki et al. 2007). All three are also detected in a space-based lensing analysis, the 3D distribution of galaxies and as extended sources in X -ray data (Hasinger et al. 2007; Finoguenov et al. 2007). Assuming the mass-luminosity relation adopted by (Finoguenov et al. 2007), the detection threshold of this very deep X -ray data is well below that expected for lensing up to redshift ~ 1 , so this acts as an ideal external arbiter (of course, X -ray mass-observable relations are somewhat uncertain). The properties of the three clusters are summarized in table 2 and demonstrate excellent agreement between the ground- and space-based data using the formalism of (Miyazaki et al. 2007).

Cluster A (SJ J0959.6+0231) is the most massive structure inside the COSMOS field, easily detected at many wavelengths. It appears to be in the process of a major merger, and has been studied individually by (Guzzo et al. 2007), who also obtained a spectroscopic redshift of $z = 0.73$. Cluster B (SL J1001.4+0159) is associated with an X -ray peak and overdensity of galaxies at $z_{\text{phot}} = 0.35$. There is a second set of galaxies at $z_{\text{phot}} = 0.85$ within $2'$, which undoubtedly complicates the interpretation a little, but our results are consistent with this high redshift projection being a minor pertur-

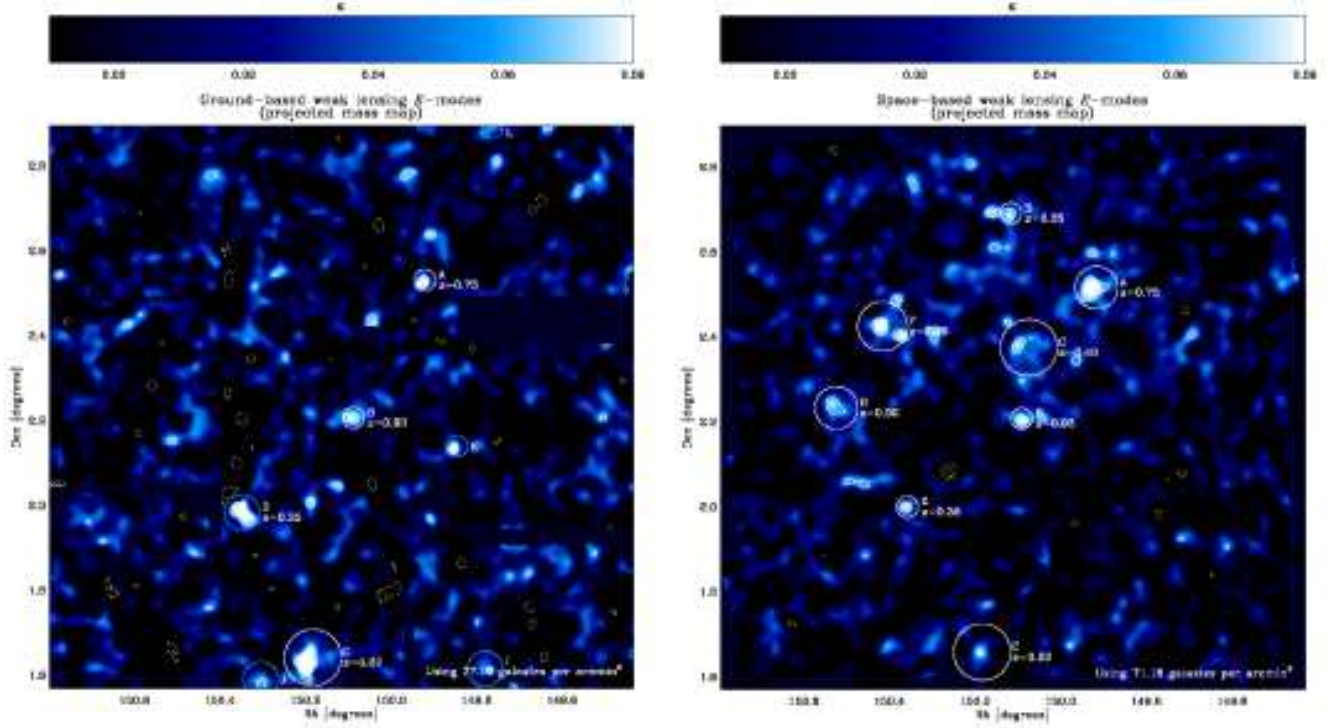


FIG. 6.— Convergence E -mode maps from the Subaru (left) and Hubble Space Telescope (right), after smoothing by a $1'$ Gaussian kernel. The data presented in the left panel are identical to that in figure 13 of (Miyazaki et al. 2007), except that the field has been slightly truncated to match the right panel. Convergence is proportional to the total projected mass along a line of sight, modulated by the lensing sensitivity function (3) plotted in figure 5. Contours are drawn at detection significances of 3σ , 4σ and 5σ , with dashed lines for underdensities. Clusters A, B, C and D are detected in both maps. Other peaks E-L are only detected in one of the two. White enclosing circles denote clusters deemed “secure” by the rigorous standards of (Miyazaki et al. 2007), and cyan circles denote “unsecure” clusters. The size of the circles shows the size of the smoothing kernel that maximises detection significance, enlarged by a factor of 2 for clarity.

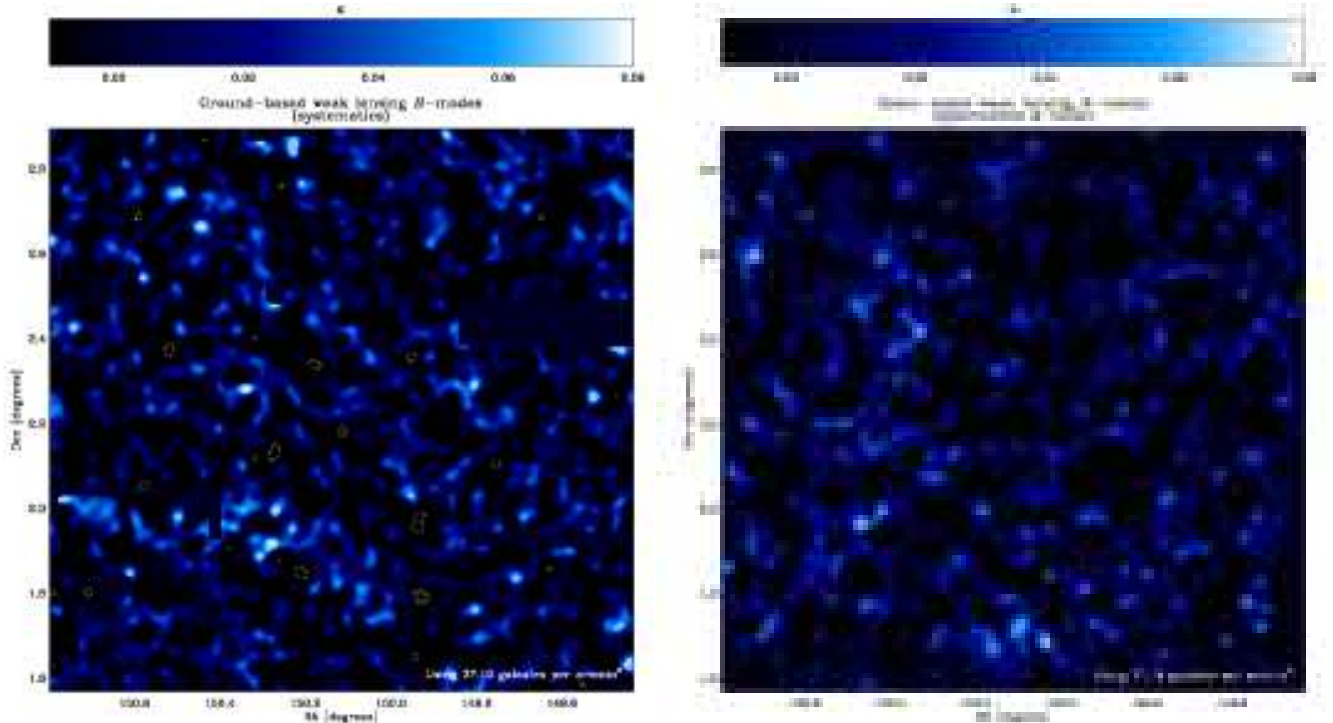


FIG. 7.— Convergence B -mode maps from Subaru (left) and Hubble Space Telescope (right) data. This is not produced by physical gravitational lensing, so deviations from zero include a combination of spurious effects from e.g. imperfect PSF correction, plus a realization of statistical noise. The smoothing scales, color ramps and contours are identical to those in figure 6.

bation. Cluster C (NSC J100047+013912) is yet more local ($z = 0.22$, Miyazaki et al. 2007) and appears large on the sky. Only part of this cluster is inside the region of HST imaging, so the space-based signal is significantly weakened, and the mass is potentially underestimated by HST.

To broaden our search, and test the limits of detectability, we additionally investigate the multi-scale procedure of (Hamana et al. 2003). For this, we smooth the convergence maps with Gaussian filters of rms width between $0.5'$ and $4'$, identifying local maxima inside the mask on each scale. For each peak with a detection signal to noise $\nu > 4$ on any scale, we record ν and the smoothing scale that maximizes ν . We also drop the restrictions on distance from the mask boundaries. This will increase the number of detected peaks, but at the expense of potentially introducing some spurious features. We then search for counterparts in the other data set, within $3'$ of detected peaks.

With the above criteria, we identify four mass peaks common to both convergence maps (A, B, C and D). Cluster D is within $3'$ of an X -ray peak, and an overdensity of galaxies at photometric redshifts $z_{\text{phot}} = 0.93$. This redshift is rather high for a lensing analysis, and it was flagged as “unsecure” by (Miyazaki et al. 2007) because it is near a boundary in the image mask. However, the tentative Subaru detection is strengthened by the confirmation from HST, and appears to be robust.

Peaks E, F, G and H (also marked on Figure 6) are seen only in the space-based map. The first three correspond to extended X -ray emission from clusters with masses M_{500} between $2 - 4 \times 10^{13} M_{\odot}$ (Finoguenov et al. 2007). Peak H is more massive ($M_{500} = 1.8 \times 10^{14} M_{\odot}$), but is at very high redshift. All four of these peaks are real detections; however no counterparts within $3'$ are seen in the ground-based map, even down to $\nu > 3$. Most likely, this is because of their lower mass and higher redshift (Hamana et al. 2003). The detection of peak G was prevented in the ground-based data by a bright foreground star.

Conversely, peaks I, J, K and L are detected only in the ground-based map. Peaks I and J are real, but lie just outside the HST imaging. There is an extended X -ray source at peak I, with unknown redshift, and a projection of two $M_{500} \approx 2 \times 10^{13} M_{\odot}$ clusters at redshifts $z = 0.40$ and $z = 0.75$ at peak J (Finoguenov et al. 2007). In both cases, there is a weak, $\nu < 3$ signal in the HST data, from the wings of the cluster. Peak K was detected in the (Miyazaki et al. 2007) analysis, but again flagged as “unsecure” because it is near the edge of a pointing. It does align with a slight, $\nu < 3$ detection in the space-based map, but there is no X -ray counterpart. This may be a spurious peak with chance coincidence, or perhaps a very distant object. Peak L appears to be spurious: such noise artifacts are more common near the edge of the field.

In summary, to the extent that we can draw conclusions from such a small sample, there is very good agreement between the primary halo catalog drawn from the ground-based data and that independently found from the space-based data. Additional halos of lower mass and higher redshift are seen in the space-based catalog, and those located uniquely in the ground-based data can

be understood in the context of either being outside the space-based region or close to its periphery.

5.3. Halo Mass Estimation

We now attempt to measure the total mass of each of the three halos (A-C) securely detected from both the ground and space. We assume that the clusters have an NFW density profile

$$\rho(r) = \delta_c \rho_c / (r/r_s)(1 + r/r_s)^2 \quad (10)$$

(Navarro, Frenk & White 1996), where δ_c is a function of the cluster’s concentration c and scale size $r_s \equiv r_{200}/c$, and r_{200} is the radius within which the mean density is 200 times the critical density. The shear profile of an NFW cluster is derived by (King & Schneider 2001). We perform a maximum likelihood fit to the log(mass) and concentration parameters, using the shear measurements from all galaxies within $10'$ of the peak convergence signal, averaged in radial bins of $0.5'$. It has been variously noted (J. Bergé, S. Paulin-Henriksson, private comm.) that fitting noisy data of individual clusters with an NFW profile does permit large (and therefore massive) models with unnaturally low concentration values. To counter this effect, we impose a concentration prior, using the lognormal distribution found for all haloes in the *Millennium Simulation* as a function of mass by (Neto et al. 2007, equations (5), (6) and figure 6). The resulting likelihood surfaces are shown in figure 8, with the effect of the prior being to close the bottom of the contours. Table 2 lists the best-fit masses and 68% confidence limits after marginalizing over concentration between $1 < c < 10$.

Although our common sample is small, there is an encouraging agreement between the detailed properties of the clusters recovered from the ground and from space. For the higher redshift cluster A, our space-based data does put significantly tighter constraints on the mass and concentration than our ground-based data. However, for the lower redshift clusters B and C, the results are satisfyingly similar. We note again that cluster C is partially outside the HST imaging. Since shears are only measured around one half of the cluster, the statistical errors in the space-based analysis are larger and its mass could be underestimated. Certainly, for massive clusters with redshifts $0.2 \lesssim z \lesssim 0.5$, it appears that our ground-based depth and resolution is adequate. The main benefit of space-based imaging is in the measurement of lower mass halos and higher redshift clusters, plus the increased resolution to further investigate the distribution of their masses.

6. DISCUSSION

We have performed parallel weak lensing analyses of Subaru and Hubble Space Telescope imaging in the COSMOS field. Our comparisons of the observed shear and convergence signals have revealed a number of issues, and suggest that such a study with real data usefully complements the independent approach based on blind analyses of simulated data (Heymans et al. 2005a; Massey et al. 2007c).

For statistical “cosmic shear” analyses, shear measurement with an existing ground based telescope, using existing measurement techniques, can be achieved

TABLE 2
CLUSTER MASSES

Cluster	RA	Dec	Redshift	XMM mass $10^{14} M_{\odot}$	HST mass $10^{14} M_{\odot}$	Subaru mass $10^{14} M_{\odot}$
A	149.917	2.515	0.73	1.90 ± 0.05	23^{+13}_{-8}	13^{+33}_{-9}
B	150.359	1.999	0.35	0.10 ± 0.01	9^{+7}_{-4}	17^{+13}_{-7}
C	150.184	1.657	0.22	1.01 ± 0.02	17^{+17}_{-9}	55^{+55}_{-27}

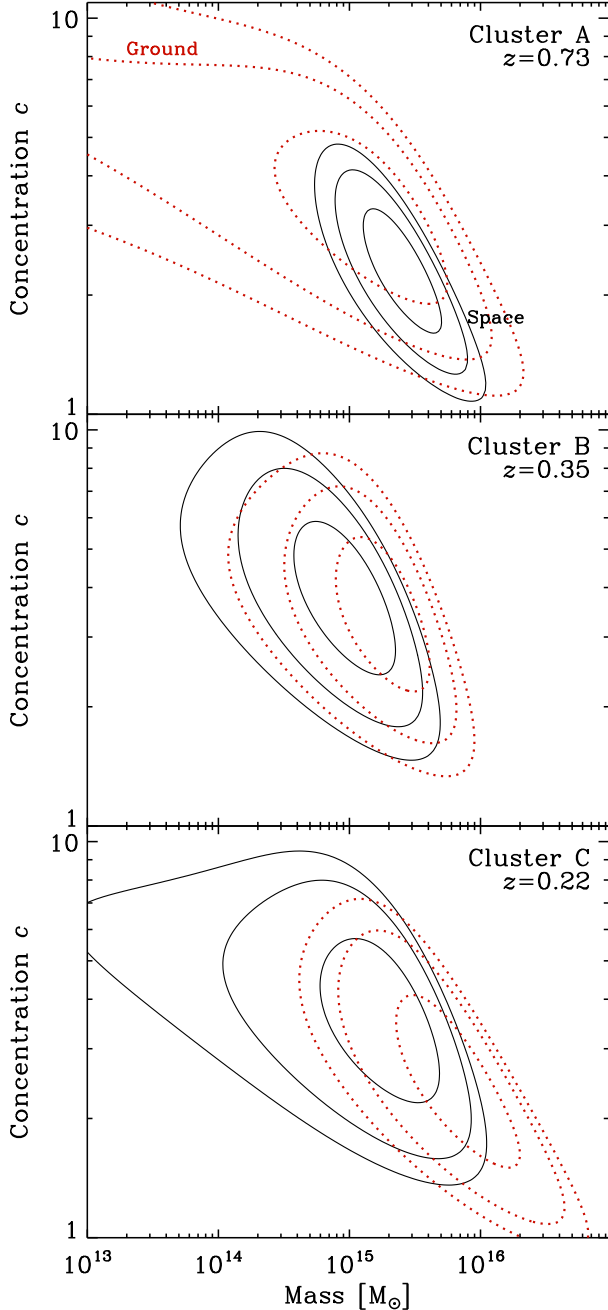


FIG. 8.— Best-fit mass and concentration index of three clusters in the COSMOS field, assuming NFW radial mass profiles. The contours show the 68%, 95% and 99% confidence regions obtained from Subaru data (dotted red) and Hubble Space Telescope data (solid black).

with less than 1% bias relative to higher resolution space-based data, for a galaxy surface density of 15 arcmin^{-2} . One limitation of our approach is that we cannot check the performance of our space-based analysis on the additional, small galaxies. At first sight the factor of ~ 3 shortfall in surface density seems inconsequential given the lower cost and improved areal mapping speed of existing ground-based cameras such as SuPrime-Cam. However, accompanying the brighter Subaru limit is a reduction in survey depth and hence the redshift distribution of background sources. More distant sources contain a larger signal, and a narrower range of redshifts also hinders tomographical tests (Bacon et al. 2005; Massey et al. 2007b), which tighten cosmological parameter constraints significantly.

A key issue is whether this limiting depth is a fundamental one for all future ground-based cameras. PanSTARRS, VST, and even LSST each have significantly smaller primary mirrors than Subaru, so achieving even the S/N discussed here would require formidable exposure times. Most importantly, the deep infrared imaging that is required for photometric redshifts to enable tomographic analyses is likely to be difficult over large survey fields from the ground, because of increased sky background. Recent weak lensing analyses are limited at roughly the same level by uncertainty in galaxy shape measurement and photometric redshift estimation.

Statistical measurements from the ground are also hindered by variable atmospheric seeing. Past experience has taught the authors that data collected in seeing worse than $0.8''$ is of little use for weak lensing analysis. The apparently rapid speed of data collection for our Subaru data belies the time spent waiting for better seeing, even with the excellent atmospheric conditions above Mauna Kea and the well-controlled dome seeing of Subaru. For this small-scale survey, we obtained exceptional quality imaging during a fortuitous observing window. The relevant quantity for larger-scale surveys in the future will be the time-averaged seeing quality, and the fraction of time spent with seeing better than $0.8''$. This is particularly true for surveys like Pan-STARRS and LSST, that plan to adopt a strategy of co-adding many shorter exposures. Their advantage is that the stacked images will achieve a near-uniform image quality, by virtue of the independent PSFs in each short exposure. This can then be tuned to the required image quality by rejecting a certain fraction of exposures.

Variable seeing conditions is also of concern for the reconstruction of mass maps (c.f. Green et al. *in prep.*). Difficulties in the analysis of one pointing in the SW corner of the Subaru map result in a patchy recovery of large-scale structure; with more noise and a lower range of probed redshift in certain regions.

Most importantly, however, the four most massive clus-

ters out of eight detected from space are also detected from the ground – with one intriguing additional signal and two more confirmed clusters just outside the field of view observed from space. Reassuringly, the three clusters conservatively deemed “secure” by the independent analysis of (Miyazaki et al. 2007) have now been confirmed via space-based weak lensing and X-ray observations. The physical properties of the four massive halos in common (A, B and C) are remarkably consistent whether derived from ground- or space-based weak lensing. The measured masses and radial profiles of these clusters are consistent and, for the lower redshift clusters, the error bars are comparable. A Dark Energy Task Force “Stage 3” survey from the ground appears eminently feasible.

A wide-field space-based platform would open up many new applications. Very important for statistical applications is the increased redshift range of resolved background galaxies. These not only contain a larger shear signal, but also more readily split into redshift bins for tomographic analysis. Three-dimensional analysis techniques will tighten constraints on cosmological parameters by factors of 3 – 5, and directly measure quantities that depend upon the properties of dark energy, like the growth of structure over cosmic time and the redshift-distance relation. They will also eliminate sources of error due to the intrinsic correlations of galaxy shapes. Sufficiently good photometric redshifts require deep, wide-field near-IR imaging, and these are also realistically possible over large surveys only from space. Recent weak lensing analyses with relatively shallow near-IR coverage like (Massey et al. 2007a) are limited to roughly the same degree by uncertainty in galaxy shape measurement and photometric redshift estimation. Full implementations of cross-correlation cosmography will almost certainly require deep near-IR imaging from space. Such advanced techniques will become particularly important as ground-based surveys expand to encompass the entire observable sky.

The increased surface density of galaxies resolved from space also improves maps of the mass distribution. As shown in figures 6 and 7, the statistical noise and systematic contamination in the *B*-mode are significantly reduced. Eight clusters are detected in the COSMOS *E*-mode signal without any contamination from spurious peaks. With the increased mass and spatial resolution of mass reconstructions from space, it becomes possible to detect halos the size of galaxy groups, as well as clusters

over a wide range of redshifts – thus tracing their formation, which is governed by the properties of dark matter and the nature of gravity. Space-based data also crosses the threshold to mapping even filamentary large-scale structure in three dimensions (Massey et al. 2007b). Obtaining the detailed, 3D distribution of mass will be particularly important near regions of interest like the Bullet cluster (Clowe et al. 2006), where the small differences between the location of mass and baryons in a small patch of sky may yield the best possible information about the properties of dark matter. In this and other astrophysical phenomena, knowledge of the local mass environment and nearby large-scale structure is critical.

Overall, we conclude that ground-based weak lensing surveys can perform several tasks remarkably well, with sufficiently small amount of systematic bias to easily justify the next generation of dedicated ground-based surveys. Two dimensional statistical analyses will be able to produce order-of-magnitude improvements in weak lensing constraints, using proven hardware technology and software pipelines. On the other hand, a wide-field space-based imager would provide important control over some systematic effects, and open up many new applications that are, at least currently, unachievable from the ground. For several of the most exciting techniques that will directly probe the nature of dark matter and dark energy, eventual space-based imaging is likely to be essential.

7. ACKNOWLEDGMENTS

This work is supported by the US Department of Energy under contract DE-FG02-04ER41316. It is based upon observations with the NASA/ESA Hubble Space Telescope, obtained at the Space Telescope Science Institute, which is operated by AURA Inc, under NASA contract NAS 5-26555. It is also based on data collected at the Subaru Telescope, operated by the National Astronomical Observatory of Japan. It is our pleasure to thank Alexie Leauthaud and Takashi Hamana for help with the catalogs and Alexandre Refregier, James Taylor and Alexis Finoguenov for useful discussions. We also gratefully acknowledge the contributions of the entire COSMOS collaboration, consisting of more than 70 scientists worldwide. More information on the COSMOS survey is available from [http://www.astro.caltech.edu/\\$\sim\\$cosmos](http://www.astro.caltech.edu/\simcosmos).

REFERENCES

- Bacon, D., Refregier, A. & Ellis, R., 2000, MNRAS, 318, 625.
 Bacon, D., Refregier, A., Clowe, D. & Ellis, R., 2001, MNRAS, 325, 1065.
 Bacon, D. et al., 2005, MNRAS, 363, 723.
 Bardeau, S., Soucail, G., Kneib, J.-P., Czoske, O., Ebeling, H., Hudelot, P., Smail, I. & Smith, G., 2007, A&A, 470, 449.
 Benjamin, J. et al., 2007, MNRAS, in press (astro-ph/0703570).
 Bernstein, G. & Jarvis, M., 2002, AJ, 123, 583.
 Bertin, E. & Arnouts, S., 1996, A&AS, 117, 393.
 Brown, M., Taylor, A., Bacon, D., Gray, M., Dye, S., Meisenheimer, K. & Wolf, C., 2003, MNRAS, 343, 100.
 Bridle, S. et al., 2001, in Scientific N. W., Proceedings of the Yale Cosmology Workshop.
 Bristow, P., 2004, ASP Conf. Proc., 314, 780.
 Capak, P. et al., 2007, ApJS, 172, 99.
 Clowe, D. et al., 2005, A&A, 451, 395.
 Clowe, D. et al., 2006, ApJ, 648, L109.
 Dahle, H., Kaiser, N., Irgens, R., Lilje, P. & Maddox, S., 2002, ApJS, 139, 313.
 Finoguenov, A. et al., 2007, ApJS, 172, 182.
 Fruchter, A. & Hook, R., 2002, PASP, 114, 144.
 Gavazzi, R. et al., 2007, A&A, 462, 459.
 Gavazzi, R. et al., 2007, ApJ, 667, 176.
 Guzzo, L. et al., 2007, ApJS, 172, 219.
 Hamana, T. et al., 2003, ApJ, 597, 98.
 Hasinger, G. et al., 2007, ApJS, 172, 29.
 Heavens, A., Kitching, T. & Taylor, A., 2006, MNRAS, 373, 105.
 Heymans, C. & Heavens, A., 2003, MNRAS, 339, 711.
 Heymans, C. et al., 2005a, MNRAS, 368, 1323.
 Heymans, C. et al., 2005b, MNRAS, 361, 160.
 Heymans, C. et al., 2006, MNRAS, 371, L60.
 Hirata, C., Seljak, U., 2003, MNRAS, 343, 459.

- Hoekstra H., Mellier Y., Van Waerbeke L., Semboloni E., Fu L., Hudson M., Parker L., Tereno I. & Benabed K., 2006, *ApJ*, 647, 116.
- Jain, B. & Seljak, U., 1997, *ApJ*, 484, 560.
- Jee, J. et al., 2007a, *ApJ*, 661, 728.
- Jee, J. et al., 2007b, *ApJ*, in press (arXiv:0705.2171).
- Kaiser N., Wilson G., & Luppino G. 2000, *ApJ*, submitted (astro-ph/0003338).
- Kaiser, N. and Squires, G. 1993, *ApJ*, 404, 441.
- Kaiser, N., Squires, G. & Broadhurst, T, 1995, *ApJ*, 449, 460.
- Kaiser, N., 2000, *ApJ*, 537, 555.
- King, L. & Schneider, P., 2001, *A&A*, 369, 1.
- King, L. & Schneider, P., 2001, *A&A*, 398, 23.
- Kitching T., Heavens A., Taylor A., Brown M., Meisenheimer K., Wolf C., Gray M. & Bacon D., 2007, *MNRAS*, 374, 1377.
- Kneib, J-P. et al., 2003, *ApJ*, 598, 804.
- Koekemoer, A. et al., 2007, *ApJS*, 172, 196.
- Kuijken, K., *A&A*, in press (astro-ph/0601011).
- Lampton, M., Sholl, M., Jelinsky, P. & Stabenau H., 2006, *AAS*, 209, 980
- Leauthaud, A. et al., 2007, *ApJ*, 172, 219.
- Mandelbaum, R., Seljak, U., Kauffmann, G., Hirata, C. & Brinkmann, J, 2006, *MNRAS*, 368, 725.
- Mandelbaum, R., Seljak, U., Cool, R., Blanton, M., Hirata, C. & Brinkmann, J, 2006, *MNRAS*, 372, 758.
- Massey, R. et al., 2004, *AJ*, 127, 3089.
- Massey, R. et al., 2007a, *ApJS*, 172, 239.
- Massey, R. et al., 2007b, *Nature*, 445, 286.
- Massey, R. et al., 2007c, *MNRAS*, 376, 13.
- Massey, R., Rowe B., Refregier, A., Bacon, D. & Bergé, J., 2007d, *MNRAS*, 380, 229.
- Maturi, M. et al., 2007, *A&A*, 462, 473.
- Mellier, Y., 1999, *Ann. Rev. Astr. Astrophys.*, 37, 127.
- Miyazaki, S. et al., 2002a, *ApJ*, 580, 97.
- Miyazaki, S. et al., 2002b, *PASJ*, 54, 833.
- Miyazaki, S. et al., 2007, *ApJ*, in press (arXiv:0707.2249).
- Mobasher, B. et al., 2006, *ApJS*, 172, 117.
- Nakajima, R. & Bernstein, G., 2007, *AJ*, 133, 1763.
- Navarro, J., Frenk, C. & White, S. 2006, *ApJ* 462, p.563.
- Neto, A. et al., 2007, *MNRAS*, submitted (arXiv:0706.2919).
- Parker, L., Hoekstra, H., Hudson, M., Van Waerbeke, L. & Mellier, Y., 2007, *ApJ*, in press (arXiv:0707.1698).
- Refregier, A., 2003, *Ann. Rev. Astr. Astrophys.*, 41, 645.
- Refregier, A. & Bacon, D., 2003, *MNRAS*, 338, 48.
- Refregier, A. et al., 2004, *AJ*, 127, 3102
- Rhodes, J., Refregier, A. & Groth, E. 2001, *ApJ*, 552, L85.
- Rhodes, J. et al., 2004, *ApJ*, 605, 29.
- Rhodes, J. et al., 2007a, *ApJS*, 172, 203.
- Schirmer, M. et al., 2007, *A&A*, 462, 872.
- Schneider, P., Van Waerbeke, L. & Mellier, Y., 2002, *A&A*, 389, 729.
- Schneider, P. 2005, *Gravitational Lensing: Strong, Weak & Micro*, Springer-Verlag, Berlin, 273.
- Schrabback, T. et al., 2007, *A&A*, 468, 823.
- Scoville, N. et al., 2007, *ApJS*, 172, 1.
- Scoville, N. et al., 2007, *ApJS*, 172, 38.
- Semboloni E., Mellier Y., van Waerbeke L., Hoekstra H., Tereno I., Benabed K., Gwyn S., Fu L., Hudson M., Maoli R. & Parker L., 2006, *A&A*, 452, 51.
- Smail I., Ellis R. & Fitchett M., 1994, *MNRAS*, 270, 245.
- Taniguchi, Y., et al. 2007, *ApJS*, 172, 9.
- Taylor, A. et al., 2004, *MNRAS*, 353, 1176.
- Van Waerbeke, L. et al., 2000, *A&A*, 358, 30.
- Wang, S. et al., 2004, *Phys. Review D.*, 70, 123008.
- Wittman, D. et al., 2000, *Nature*, 405, 143.
- Wittman, D. et al. 2005, *ApJ*, 632, 5.
- Wittman, D., Dell’Antonio, I., Hughes, J., Margoniner, V., Tyson, J., Cohen, J. & Norman, D., 2006, *ApJ*, 643, 128